Journal of Power Sources 335 (2016) 189–196

Contents lists available at ScienceDirect

Journal of Power Sources

journal homepage: www.elsevier.com/locate/jpowsour

The effect of charging rate on the graphite electrode of commercial lithium-ion cells: A post-mortem study

L. Somerville [a, b], J. Bareño [a], S. Trask [a], P. Jennings [b], A. McGordon [b], C. Lyness [c], I. Bloom [a, *]

[a] Argonne National Laboratory, 9700 S. Cass Ave., Lemont, IL 60561, USA
[b] WMG, University of Warwick, Coventry, England CV4 7AL, UK
[c] Jaguar Land Rover, Banbury Road, Warwick, England CV35 0XJ, UK

HIGHLIGHTS

- Higher charging currents increase the quantity of negative electrode surface film.
- Degradation preferentially occurs along the center of the electrode roll.
- This degradation is related to insufficient electrode wetting.
- The center of the electrode roll delaminates at rates of 6-C.
- Delamination is caused by binder degradation from increased temperature.

ARTICLE INFO

Article history:
Received 29 July 2016
Received in revised form
27 September 2016
Accepted 3 October 2016
Available online 22 October 2016

Keywords:
Lithium-ion
Increased charge rate
Aging
Materials characterization

ABSTRACT

Increased charging rates negatively affect the lifetime of lithium-ion cells by increasing cell resistance and reducing capacity. This work is a post-mortem study of 18650-type cells subjected to charge rates of 0.7-, 2-, 4-, and 6-C. For cells charged at 0.7-C to 4-C, this performance degradation is primarily related to surface film thickness with no observable change in surface film chemical composition. However, at charge rates of 6-C, the chemical composition of the surface film changes significantly, suggesting that this change is the reason for the sharper increase in cell resistance compared to the lower charge rates. In addition, we found that surface film formation was not uniform across the electrode. Surface film was thicker and chemically different along the central band of the electrode "jelly roll". This result is most likely attributable to an increase in temperature that results from non-uniform electrode wetting during manufacture. This non-uniform change further resulted in active material delamination from the current collector owing to chemical changes to the binder for the cell charged at 6-C.

1. Introduction

A common criticism of electric vehicles is that they have a much smaller range compared to those with a traditional internal combustion engine (ICE). Electric vehicles typically have a range of 100–300 km between charges, whereas ICE vehicles have a range of 800–1000 km. In addition, it takes approximately five minutes to refill an ICE vehicle's tank, whereas recharging electric vehicles can take up to eight hours. This difference in charge/refill time presents a significant barrier to consumer acceptance of electric vehicles.

The reason electric vehicles take longer to charge is because the lifetime (capacity and power) of the cell is significantly reduced as the charging rate increases. Previous work into this area has shown the negative impact of charge rate on cell performance [1].

When a cell is being charged, lithium-ions transfer out of the positive electrode; pass through the electrolyte; and intercalate into the negative electrode. Charging rate is the speed at which this transfer takes place. Increased current rate increases the amount of lithium plating onto the negative electrode surface [2,3]. Lithium plating is accelerated by three conditions, these are low temperature [4], increased current rates during charge [3] and high state of charge [5]. Smart and Ratnakumar explain that lithium plating

* Corresponding author.
E-mail address: ira.bloom@anl.gov (I. Bloom).

http://dx.doi.org/10.1016/j.jpowsour.2016.10.002

occurs because of two competing mechanisms [6]. These are intercalation into the electrode and plating onto the electrode surface. At low temperatures the kinetics of intercalation are hindered and as a consequence lithium plates onto the surface of the electrode. At increased current rates the negative electrode is polarised to a lower potential and the mechanism of intercalation is superseded by lithium plating. This is because at below 0.0 V (vs Li/Li^+) lithium preferentially plates onto the negative electrode [7] instead of intercalating into the graphite.

Increased charge rate has also been related to thickening surface film [8,9] and blocking electrode pores [10]. Both of these are outcomes of lithium plating at the negative electrode. By increasing the concentration of lithium at the surface of the electrode, reduction of the electrolyte will occur more rapidly because the concentration of reactants has increased. Zhang postulates that when the Li^+ ion intercalation paths become blocked, it increases the concentration at other paths [3]; this finding further increases the localized current rate at the other pores, which, in turn, increases the rate of lithium plating.

There is some ambiguity because these conclusions are based on models, electrical data, and/or theoretical calculations alone. Plus, the behavior of commercial cylindrical format cells can often differ from that of laboratory coin cells. If we knew which chemical mechanisms were responsible for the cell's degradation in commercial cells, it may be possible to mitigate them and increase battery life through better cell control or material design. This work utilizes analytical methods to study the internal materials of commercial 18650-type cells after the cells were subjected to varied rates of charge to determine the location, extent, and cause of damage. This study is the first of its type to quantify the relationship between electrical performance and internal chemical changes from commercial cells subjected to different rates of charge.

2. Experimental

2.1. Materials

Twelve commercially available 1.25Ah NiMnCo/graphite 18650-type cells were charged between 0 and 100% state of charge at rates of 0.7-, 2-, 4-, and 6-C, respectively (three cells at each charge rate). All cells were discharged at a rate of C/3. The cells were cycled in temperature-controlled environmental chambers at 25 °C and allowed to rest for 30 min after each charge and discharge [11].

For post-mortem analysis, the cells were discharged to 0.5 V. They were dismantled in an argon-filled glove box. The cathode/separator/anode roll was unwound, and samples were cut from the bulk of the electrode material using stainless steel scissors. Care was taken to handle the samples with tweezers by the edges, and samples were stored separately in individual re-sealable plastic bags.

2.2. Characterization

After unwinding and harvesting the electrodes in a glove box, samples were transferred to an adjoining glove box via a common antechamber for analysis. During this transfer, samples were exposed to pressures of around 1.0×10^{-4} kPa for 15 min but were not exposed to air.

Scanning electron microscope (SEM) samples were transferred to the microscope using a custom-made, air-tight sample holder, which was adapted from that used by Howe et al. [12]. Micrographs were collected on a JEOL JSM 6610LV scanning electron microscope using an accelerating voltage of 10 kV and a working distance of 15 mm with a secondary electron detector.

X-ray photoelectron spectroscopy (XPS) samples (10 × 10 mm) were mounted on a sample holder by means of double-sided tape. Spectroscopy was performed using a Physical Electronics 5000 VersaProbe II with a monochromatic aluminum Kα (15 kV) X-ray source. The excitation beam size employed was 100 μm, and the power was 25 W. Pressures of the system were between 2×10^{-10} kPa before sample insertion and 2×10^{-9} kPa immediately after. Ar^+ ion sputtering was performed at 500 V over an area of 3 × 3 mm F1s spectra were recorded in Fixed Analyzer Transmission mode, using a pass energy value of 11.75 eV, step size of 0.1 eV, and acquisition time of 2.7 s/step. Binding energy correction was carried out assuming that the main component of the C1s region after sputtering corresponds to C—C (graphite) environments at 284.4 eV.

High performance liquid chromatography (HPLC) was performed with an Agilent Technologies 1260 infinity series liquid chromatograph containing a 6120 Quadrupole mass spectrometer. The stationary phase was three Agilent Technologies oligopore 5 μm columns, with HPLC quality methanol (MeOH) (90%) and water (10%) as the mobile phase; the tests were performed at 25 °C. HPLC samples were created by washing the electrode in the glove box with 5 mL of dimethyl carbonate (DMC), and ~0.1 g of calcium carbonate ($CaCO_3$) was added afterward. The samples were then transferred out of the glove box and mixed vigorously with 5 mL of water. The organic phase was then extracted by syringe and filtered twice with grade 5 Whatman filter paper soaked in DMC. The sample was desiccated overnight and then re-solvated with 2 mL of dichloromethane (DCM).

3. Results

The electrical performance of these cells was presented in an earlier paper by Prezas et al. [11]. Briefly, as the charge rate increased, the cell resistance increased and the capacity reduced. In this work, these cells were dismantled to understand the underlying changes that caused the performance decline.

Fig. 1 depicts the negative electrodes at each charge rate based on a photograph in Ref. [11]. The electrodes in an 18650-type cell are stacked on top of one another with a separator between them. This is then rolled up like a scroll to form the jelly roll that sits inside the can. The illustration of the electrodes in Fig. 1 is a cross section of that jelly roll. The electrodes, as illustrated in this figure by the cell can, align with the top and bottom of the 18650 can as they are positioned within the can during use. The middle refers to the part of the electrode furthest from both the bottom and top of the can. The 0.7- and 2-C electrodes look identical in color, shading, and appearance. The 4-C electrode is mostly similar in color and appearance but has a single grey band covering approximately one-third of the middle of the electrode roll. The electrode from the cell subjected to a charge rate of 6-C also has a band; however, it covers only one-quarter of the electrode, and the active material is delaminated from the current collector so that the copper is visible in places within this band. The presence of the grey-colored band in the center of the 4-C charged electrode and the delamination along the center of the 6-C charged electrode indicates that the increased charge rate is affecting the middle sections at the 4- and 6-C rates of charge differently. This difference is highlighted further by Fig. 1 inset, which is a magnified photograph of the 6-C electrode and shows that the electrode changes in color across the electrode surface. It is multicolored with white patches in the middle (far right), and moving from the middle to the outside of the electrode (far left), the color changes from greenish to blue to lighter blue to grey. Although chemical changes in surface film do not always present themselves visually, changes in color always indicate a change in the thickness or chemistry of the material under study.

Delamination of the 6-C electrode had a uniform pattern in the

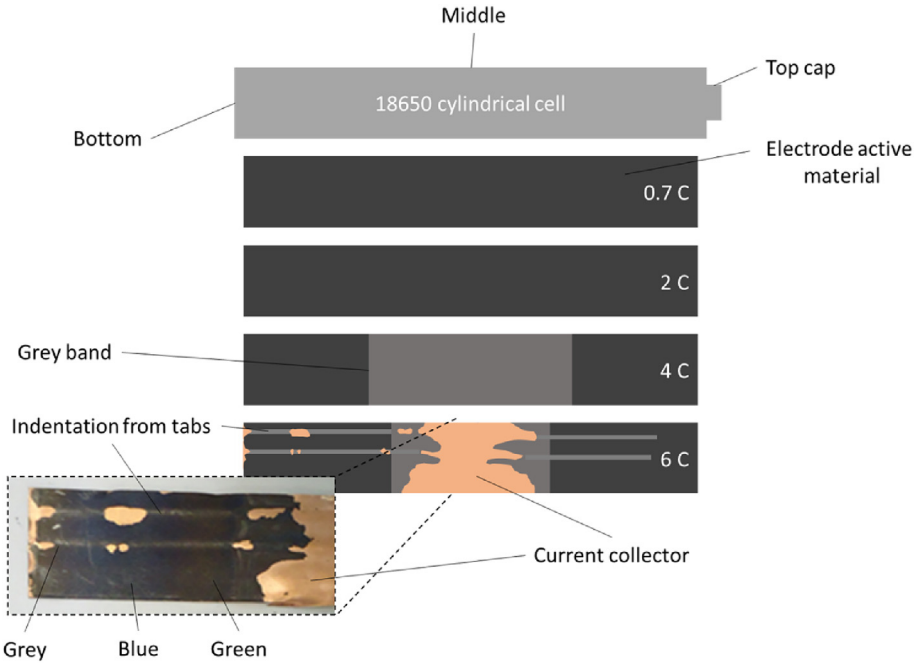

Fig. 1. Graphic of graphite electrodes from commercial 18650-type lithium-ion cells that have been subjected to different rates of charge (0.7-, 2-, 4-, and 6-C). The photograph (inset) shows one side of the 6-C electrode. Original photographs of the graphic can be found in Ref. [11]. The electrodes shown are cross sections and the position of damage caused by fast charging relates to the same position on the electrode as in the can labelled middle, top cap and bottom.

center and across the length of the electrode roll. This pattern of delamination comes in and back out like two opposing sinusoidal waves. Part of this pattern is caused by lines in the electrode material running from the bottom of the can to the top cap that are repeated in an almost equidistant pattern along the length. These lines perfectly aligned with the current collector tabs when the electrode is rolled up, which were at either end of the negative electrode (two) and in the middle of the positive electrode (one).

It should be noted that the delamination observed in the 0.7-, 2-, and 4-C cells was random and therefore related to the opening of the cell and not to the operating conditions, whereas the other features mentioned were consistent across the electrode surface and in multiple cells.

3.1. SEM

Fig. 2 contains micrographs of the negative electrodes from cells charged from 0.7-C to 6-C. These images are from both the middle and the outside (close to the top cap/bottom) of the electrode roll. There are two key points to be made. First, the outside part of the roll for the 0.7-C and 2-C charged electrodes' active material looks like pristine graphite. At 4-C, small, lighter-colored dots are present, and at 6-C, it is more difficult to identify individual graphite particles because of a surface film. In contrast to this apparent trend of the outside electrode images, it is clear that the middle of the electrode roll does not appear to be pristine graphite at any rate of charge and instead has a film covering the graphite particles. A trend is not clear, using SEM, of the extent of surface film growth on the inner track of the electrode roll as it is for the outer track. However, the inside track has a greater amount of surface film than that on the outside in each case except for 6-C, which is visually similar for both the middle and outside.

3.2. HPLC

Fig. 3 is the liquid chromatogram of the surface film removed

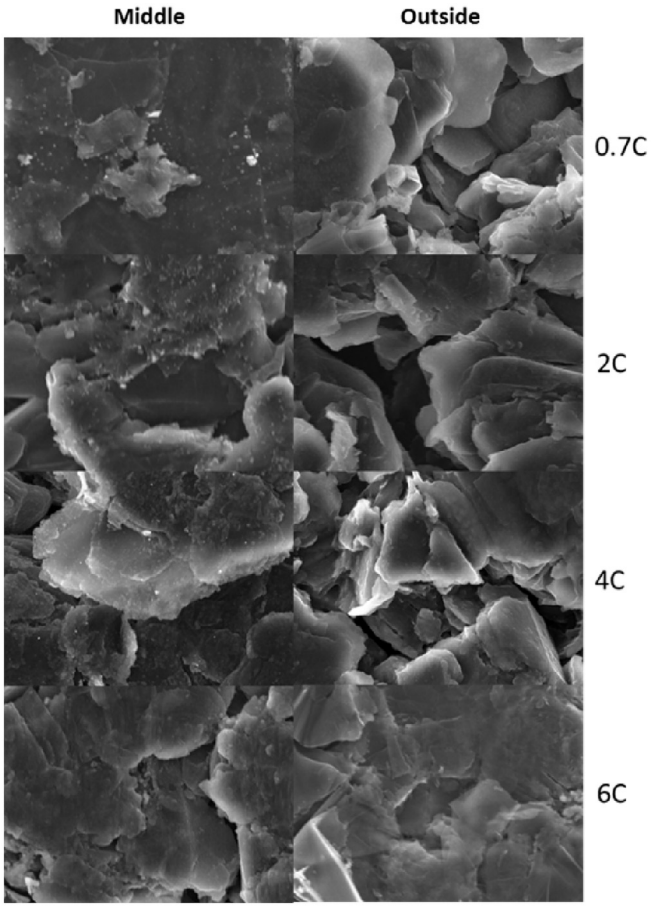

Fig. 2. Micrographs of graphite electrodes from commercially available 18650-type cells that were subjected to different rates of charge (0.7-, 2-, 4-, and 6-C). The "Middle" and "Outside" labels refer to micrographs taken furthest from the top cap and bottom of the 18650 size cell (Middle) and those taken closest to them (Outside).

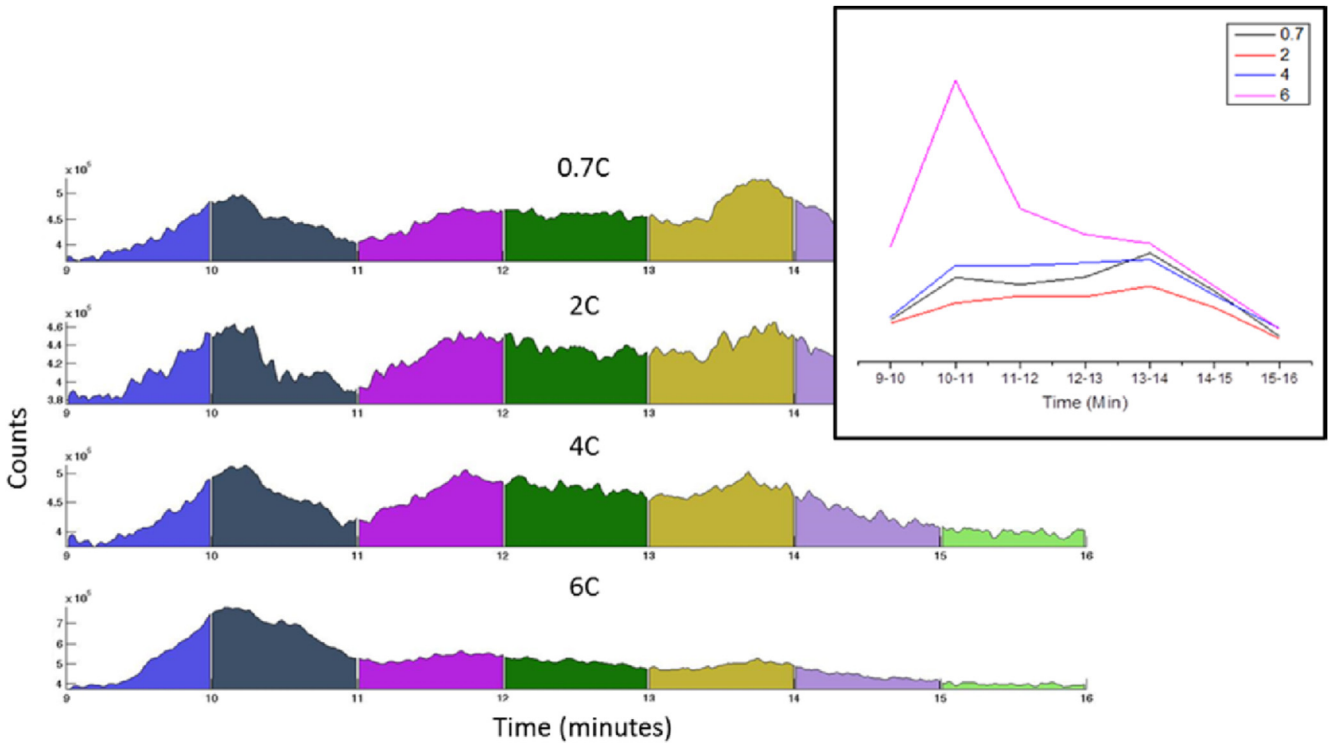

Fig. 3. High-performance liquid chromatography of electrode surface film removed from cells that have been subjected to different rates of charge (0.7-, 2-, 4-, and 6-C). The inset is the integration of the total counts for each 2-min period.

from the electrodes at each C-rate from samples cut into the middle of the electrode material. Fig. 3 inset shows the total intensity within each minute (marked by color bands).

The authors are not aware of any work that has used HPLC to study the polymerized component of the surface film in commercial lithium-ion cells; this is due to the likelihood of forming hydrogen fluoride (HF) from the reaction of lithium hexafluorophosphate ($LiPF_6$) with moisture. Petibon et al., present a method of liquid-liquid extraction for preparation of samples for gas-chromatography [13]. The method in our work contains $CaCO_3$ to ensure that formation of HF does not impact the surface films chemical composition. We created a method to selectively react with and then remove the $LiPF_6$ component. However, surface film of lithium-ion cells contains many polymeric components with varied masses, and therefore it was not possible to resolve each separately. This method instead integrates one-minute intervals to determine differences in chemical composition between samples.

The 0.7-, 2-, and 4-C electrodes are almost identical. In contrast, the 6-C electrode is considerably different, containing much higher concentrations in the 9–10- and 10–11-min time intervals. The size exclusion columns used elute higher molecular weight (MW)/more branched oligomers soonest and lower MW, less-branched oligomers later. Therefore, the 6-C electrode had a higher concentration of the higher MW oligomers compared to the others. This finding suggests that the surface film of the 6-C electrode is chemically different from those at other C-rates. The plots are almost identical at less than 9.5 min and after 14 min, indicating that this difference is mainly from the addition of a greater concentration of higher MW oligomers only and not through creation of different molecules.

3.3. XPS

Fig. 4 shows the XPS spectra of the C1s spectra of the outside of the electrodes at each C-rate. The 0.7-C to 4-C spectra peak positions align almost perfectly, whereas the 6-C electrode's C–O peak requires an adjustment of 0.6 eV to lower binding energy to allow for a probable change in chemical environment and also an increase in its FWHM (full width at half maximum) of 0.5 eV. In contrast, the others are almost identical in peak position and FWHM values (<0.1 eV variance). The assignment of peaks is according to previous work [14,15].

Fig. 5 presents the relative peak areas for each chemical environment (a) and for all C–C graphite and non C–C graphite peaks (b). Fig. 5a shows that as the C-rate increases, the percentage of C–C graphite decreases, whereas the concentration of C–O and O–C=O species increase. The concentration of RO_2CO_2Li species remains between 0% at 0.7-C and 8% at 2-C but does not show a trend with C-rate. When the sum of these non-graphite environments (C–O, O–C=O, and RO_2CO_2Li) is compared to the C–C graphite environments (Fig. 5b), we can see an increase in surface film as the C-rate increases. At 6-C, the concentration of surface film to graphite is 57% surface film to 43% graphite. In each case, as the C-rate increases, so too does the concentration of surface film compared to graphite.

Fig. 6 shows the C1s spectra of the middle and outside of the 2-C electrode. The findings indicate that there is a chemical difference. The O–C=O component is not present on the outside, whereas it is present in the middle. In addition, the contributions of both C–O and RO_2CO_2Li increase significantly in the middle as compared to the outside. The graphite reduces from 62% on the outside to 39% on the inside, a reduction of approximately one third and an increase in surface film of one half. The shift of the C–O and RO_2CO_2Li peaks to a lower binding energy suggests that the surface film containing these groups is reduced. XPS shows that the inside contains a greater quantity of surface film compared to the outside. This same trend, shown here for 2-C electrodes, was consistent across C-rates. The inside always contained a much higher quantity (>20%) of

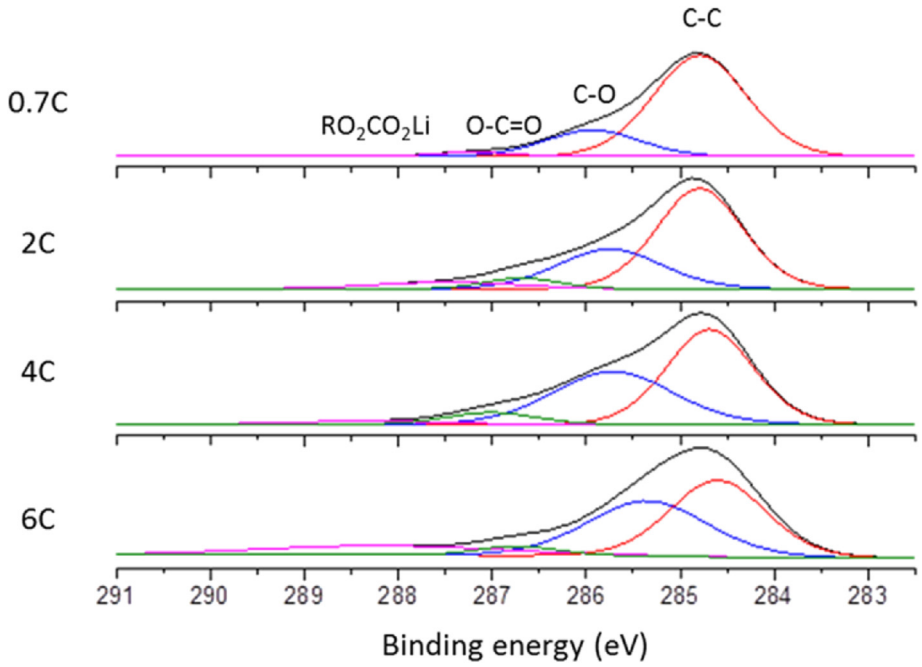

Fig. 4. C1s XPS spectra of graphite electrodes after sputtering from commercial 18650 cells subjected to different rates of charge (0.7-, 2-, 4-, and 6-C).

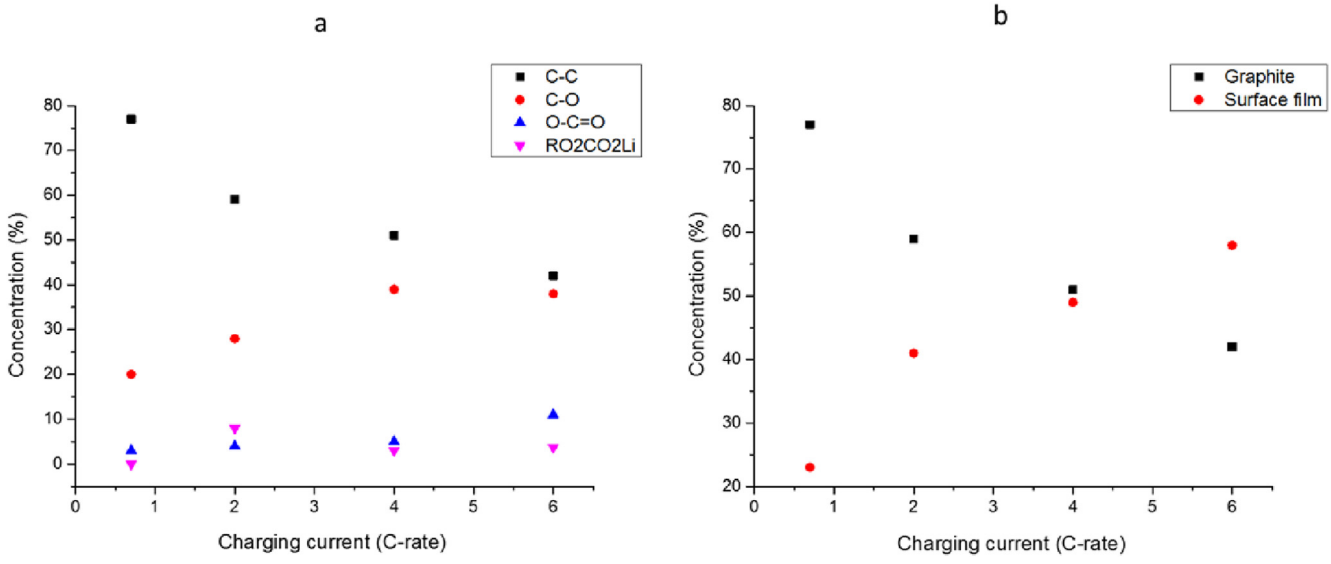

Fig. 5. (a) The peak areas plotted as a percentage of total C1s environments taken from Fig. 4 and (b) the sum of all non C–C environments (surface film) compared to all C–C environments.

surface film as compared to the outside.

4. Discussion

This work has shown that there are two effects that occur during the fast charging of lithium-ion cylindrical cells. These are the impact that the rate of charging has on the electrode and the difference in the material between the middle and outside of the electrode roll. Because of this distinction, the discussion addresses these issues separately.

4.1. Effect of charging rate on the middle compared to the outside of the electrode roll

The photographs and micrographs show that as the C-rate increased, it had a different impact on the middle track of the electrode roll than on the outside. Although this effect is most pronounced for the 6-C electrode that had delaminated in places, the 4-C electrode similarly had a grey band in the middle. The micrographs show that although not visually observable, the C-rate had consistently increased the concentration of surface film more in the middle than on the outside. While it was not possible to see any surface film in the micrographs on the outside track of the cells charged at 0.7- and 2-C, the middle track showed that surface film

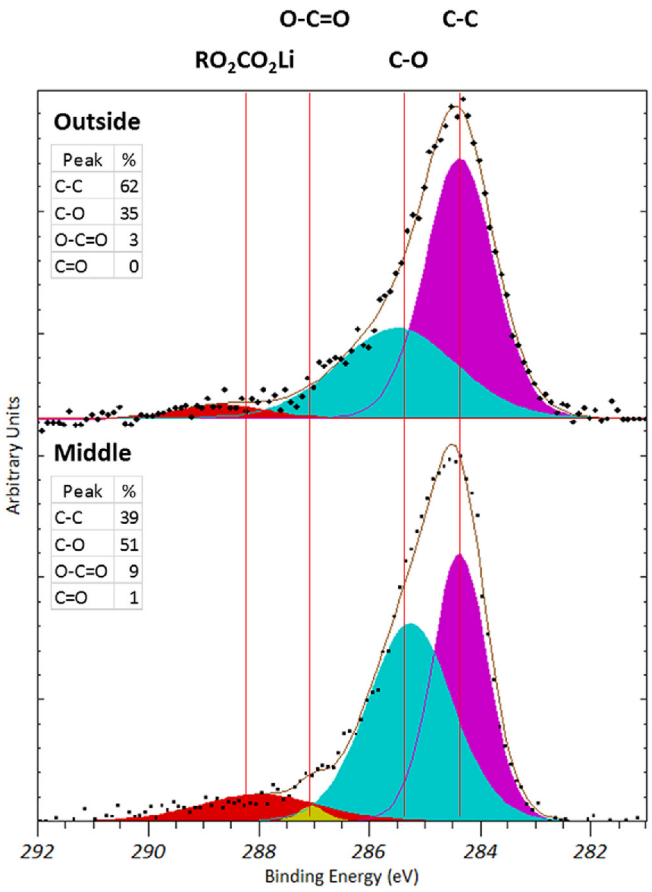

Fig. 6. C1s XPS spectra of a graphite electrode from a cell subjected to charge rate of 2-C. The inside refers to the electrode furthest from the top and bottom of the 18650-size cell, whereas the outside refers to the electrode closest to the top or bottom of the electrode roll.

was covering the graphite particles—so it was often difficult or impossible to differentiate between them. Fig. 6 supports this finding by showing that the surface film component of the middle of the electrode roll was 150% greater than that on the outside. This increase in surface film cannot be a consequence of the current path preferentially moving along the inside track. The current collector tabs were located at both ends of the unrolled negative electrode and in the center of the positive electrode. Therefore, a preferred current path is not the reason why this surface film would be most pronounced along the center.

A possible reason for this increase in surface film along the middle of the electrode roll is presented in the work of Wood et al. [16]. They note that wetting of the electrode roll during cell manufacture is a “bottleneck” to the formation and manufacture of lithium-ion cells: this step in the manufacturing process can take a long time because incorrect wetting significantly increases both localized surface resistance and overall cell resistance. The wetting process involves the injection of electrolyte both on top of the jelly roll and down to the bottom of the cell and through the mandrel hole. This step is performed multiple times in an attempt to ensure that sufficient electrolyte is capable of reaching the middle. Reeves and Morris [17] note that an electrode's active material that is not sufficiently wetted increases in both electronic and charge transfer resistance, significantly affecting the SEI film formation and overall cell resistance.

The conclusions of these authors are in keeping with the results of this present study. As charging rates increase, insufficient electrolyte wetting along the middle of the electrode roll causes impedance to increase. At 2-C and above this becomes a critical issue because it may comprise a large proportion of the cells total resistance increase which in turn increases surface film formation. This mechanism is likely to become self-propagating, as resistance increases, so will temperature and thus the localized rate of diffusion increases, further increasing surface film formation. This mechanism is not likely to be seen in a laboratory coin cell, small pouch cells, and possibly even large-format cells.

4.1.1. Delamination

At much higher C-rates (6-C), we found that the electrode active material in the middle had delaminated in places. This delamination was most pronounced in the very middle of the electrode roll but also had a very specific pattern. This pattern of delamination moving in and then back out was most pronounced when in line with the current collector tabs. Fig. 1 shows that at each point at which the tab has been positioned, the delamination moves further out from the middle. Because the delamination only occurs along the middle of the electrode roll and is most pronounced when it aligns with the tabs, the most likely explanation is that it is caused by an increase in temperature. It is well known that the tabs are the hottest parts of the cell because they are subjected to higher current. Therefore, at 6-C, the temperature of the middle of the electrode roll (which is hotter due to wettability issues) increases significantly so that the binder properties are negatively affected. This finding is consistent with the much steeper decrease in cell electrical performance at 6-C as noted in Ref. [11].

We tested this hypothesis by placing samples of electrode material cut from the outside and the middle of the cell subjected to 6-C into electrolyte solution and stored in environmental chambers at various temperatures. Photographs from this test are shown in Fig. 7. The electrode from the outside of the cell maintained adhesion at 30 °C (Fig. 7a), whereas the electrode from the middle delaminated at 30 °C (Fig. 7b) and turned to paste at 55 °C (Fig. 7c). The increase in temperature permanently affected the chemical properties of the binder such that it reduced its adhesion to the current collector.

The increase in surface film and delamination of the 6-C cell are linked to the same underlying cause. This cause is likely to be insufficient electrolyte wetting of the middle band, which causes an increase in temperature, further lithium plating (although not explicitly shown in our work), and electrolyte reduction, as shown by the shift in C—O and RO_2CO_2Li peaks to a lower binding energy in the C1s spectra. It is our conclusion that at 6-C, the rate of intercalation, lithium plating, and resistance all increase such that the binder is damaged, causing delamination of the electrode's active material from the current collector along this middle band.

4.2. Effect of C-rate on the graphite electrode surface film

Micrographs of the outside track of the electrode roll show that as the charging rate increases from 2-C to 4-C, the graphite loses its pristine look. By 6-C, the graphite particles are indistinguishable from one another because of an increase in surface film and/or electrolyte deposits. This trend in which there is a significant difference in the surface films of the 4-C and 6-C electrodes is also shown by the HPLC results in Fig. 3. At 6-C, the quantity of higher MW/more branched oligomer compounds increases significantly. The higher C-rate surface film is composed of a higher concentration of these compounds, which appears to have affected the resistance of the cell as a consequence.

XPS shows that C-rate increases the quantity of surface film present. As the C-rate increases, the surface film thickens. A change in the chemical composition of the electrode is supported by Fig. 4,

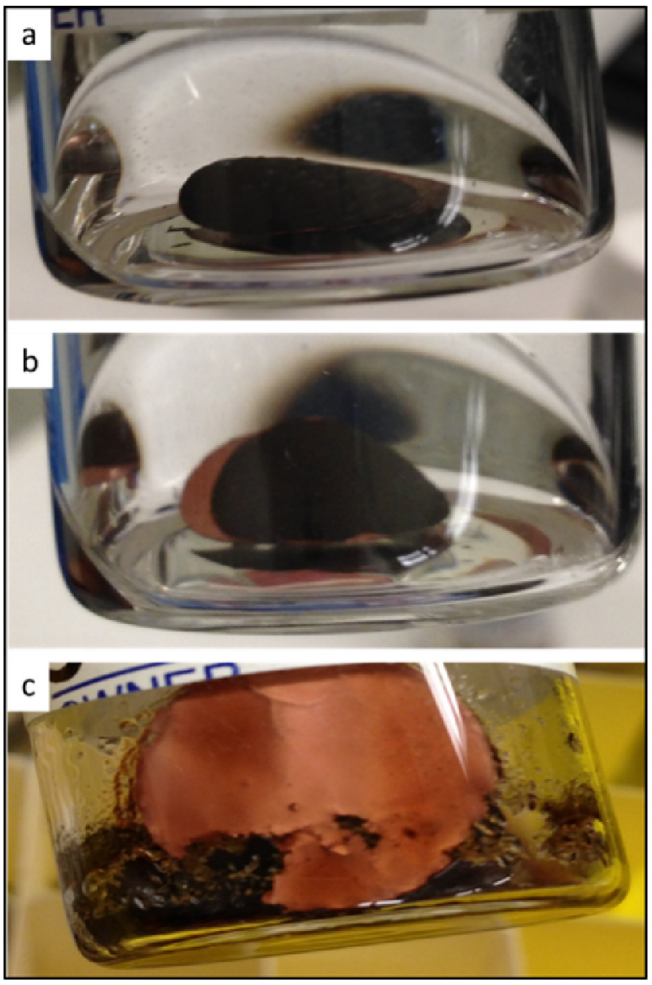

Fig. 7. Photographs of graphite electrodes cut from commercial cylindrical cells from the outside (a) and inside (b and c) of the electrode roll immersed in electrolyte and stored at 30 °C (a and b) and 55 °C (c).

which shows how the 0.7-C to 4-C electrode chemical environments maintain approximate peak shape and position, whereas the 6-C cell does not. The 6-C surface film is chemically different as a result of electrolyte reduction with respect to the others.

The change in total percentage of graphite environments to surface film values (Fig. 5) shows that as the C-rate initially increases from 0.7-C to 2-C, the rate of surface film growth doubles from ~20% to ~40%. This rate of increase then slows down so that the rate of surface film increases to ~48% at 4-C and then to 57% at 6-C. Our work is in agreement with Gallagher et al. [18] who calculated that at or above 4 mA/cm^2, additional deleterious side reactions occur. The cells within this study had an active material loading equating to approximately 3.7 mA/cm^2 at a charge rate of 1-C. These results support Gallagher et al.'s work because of the sharp increase in resistance and surface film thickness between 0.7-C and 2-C. In addition, it shows that these deleterious reactions cause the same reactions to occur at a faster rate, thickening the surface film and not chemically altering its composition. Please note the cells used in these tests were commercially available, and, as such, the current density value is based on the measured electrodes and nominal capacity of the cell at the time of opening. It is therefore only approximate.

5. Conclusions

The charging rate increases the percentage concentration (thickness) of surface film from ~20% at 0.7-C to ~57% at 6-C. The relation of this surface film to resistance increase can be correlated to the surface film thickness at between 0.7-C and 4-C. However, at 6-C, the chemical composition of the surface film changes and so additional resistance increases may be associated with this chemical change, in addition to surface film thickness increases.

The charge rate does not affect the electrode uniformly. The electrode surface film increases significantly along the middle band of the electrode, and this finding is most likely to result from non-uniform wetting of the electrode with electrolyte during manufacturing. This condition creates an increase in surface film at all rates of charge but, in addition, causes delamination of the electrode from the current collector at a charge rate of 6-C. This delamination is related to temperature caused by a rise in resistance along this central band.

This work provides experimental and quantifiable evidence of the impact of current rate during charge on the negative electrode. Knowing the surface film's relative thickness and points of chemical change may help in modeling surface film growth for further work to improve charge rates for lithium-ion cells in the future. It also shows that electrode wetting is a possible cause for the discrepancies observed between charge rates of cylindrical cells.

Acknowledgements

We acknowledge support from the Engineering and Physical Sciences Research Council (EPSRC) (EP/I01585X/1) and the WMG centre HVM Catapult. We also acknowledge support from Jaguar Land Rover Automotive PLC.

The work at Argonne National Laboratory was performed under the auspices of the U.S. Department of Energy (DOE), Office of Vehicle Technologies (VTO), under Contract No. DE-AC02-06CH11357.

The submitted issue has been created by the University of Chicago as Operator of Argonne National Laboratory ("Argonne") under Contract No. W-31-109-Eng-38 with the U.S. Department of Energy. The U.S. Government retains for itself, and others acting on its behalf, a paid-up, non-exclusive, irrevocable, worldwide license in said article to reproduce, prepare derivative works, distribute copies to the public, and perform publicly and display publicly, by or on behalf of the Government.

Glossary

$CaCO_3$	calcium carbonate
DMC	dimethyl carbonate
FWHM	full width at half maximum
HF	hydrogen fluoride
ICE	internal combustion engine
$LiPF_6$	lithium hexafluorophosphate
MW	molecular weight
r.d.s.	rate-determining step
SEI	solid electrolyte interphase
SEM	scanning electron microscopy
XPS	X-ray photoelectron spectroscopy

References

[1] X. Han, M. Ouyang, L. Lu, J. Li, Y. Zheng, Z. Li, J. Power Sources 251 (2014) 38–54.
[2] W.R. Bennett, Energytech, 2012 IEEE, IEEE, 2012, pp. 1–5.
[3] S.S. Zhang, J. Power Sources 161 (2006) 1385–1391.
[4] H.-P. Lin, D. Chua, M. Salomon, H. Shiao, M. Hendrickson, E. Plichta, S. Slane,

Electrochem. Solid State Lett. 4 (2001) A71–A73.
[5] V. Agubra, J. Fergus, Materials 6 (2013) 1310–1325.
[6] M. Smart, B. Ratnakumar, J. Electrochem. Soc. 158 (2011) A379–A389.
[7] J. Burns, D. Stevens, J. Dahn, J. Electrochem. Soc. 162 (2015) A959–A964.
[8] S.S. Choi, H.S. Lim, J. Power Sources 111 (2002) 130–136.
[9] W. Lu, C.M. López, N. Liu, J.T. Vaughey, A. Jansen, D.W. Dees, J. Electrochem. Soc. 159 (2012) A566–A570.
[10] M. Broussely, P. Biensan, F. Bonhomme, P. Blanchard, S. Herreyre, K. Nechev, R.J. Staniewicz, J. Power Sources 146 (2005) 90–96.
[11] P.D. Prezas, L. Somerville, P. Jennings, A. McGordon, J. Basco, T. Duong, I. Bloom, SAE Technical Paper, 2016.
[12] J.Y. Howe, L.A. Boatner, J.A. Kolopus, L.R. Walker, C. Liang, N.J. Dudney, C.R. Schaich, J. Mater. Sci. 47 (2012) 1572–1577.
[13] R. Petibon, L. Rotermund, K. Nelson, A. Gozdz, J. Xia, J. Dahn, J. Electrochem. Soc. 161 (2014) A1167–A1172.
[14] R. Dedryvère, S. Laruelle, S. Grugeon, L. Gireaud, J.-M. Tarascon, D. Gonbeau, J. Electrochem. Soc. 152 (2005) A689–A696.
[15] S. Leroy, F. Blanchard, R. Dedryvere, H. Martinez, B. Carre, D. Lemordant, D. Gonbeau, Surf. Interface Anal. 37 (2005) 773–781.
[16] D.L. Wood, J. Li, C. Daniel, J. Power Sources 275 (2015) 234–242.
[17] S. Reeves, R.S. Morris, Electrochem. Solid State Lett. 7 (2004) B29–B30.
[18] K.G. Gallagher, S.E. Trask, C. Bauer, T. Woehrle, S.F. Lux, M. Tschech, P. Lamp, B.J. Polzin, S. Ha, B. Long, J. Electrochem. Soc. 163 (2016) A138–A149.